Key Engineering Materials
ISSN: 1662-9795, Vol. 926, pp 1083-1092
doi:10.4028/p-71zvp8

Submitted: 2021-12-20
Revised: 2022-01-25
Accepted: 2022-02-04
Online: 2022-07-22

Investigation of the Tube Expansion Test with Elastomer Using Locally Overaged AA6063 Tubes

Antonio Piccininni[1,a], Maria Beatriz Silva[2,b*] and Gianfranco Palumbo[1,c]

[1]Department of Mechanical Engineering, Mathematics & Management Engineering, Division of Production Technologies, Polytechnic University of Bari, via Orabona 4, 70125 Bari, Italy

[2]IDMEC, Instituto Superior Técnico, Universidade de Lisboa, Av. Rovisco Pais, 1049-001 Lisboa, Portugal

[a]antonio.piccininni@poliba.it, [b]beatriz.silva@tecnico.ulisboa.pt, [c]gianfranco.palumbo@poliba.it

Keywords: locally overaged tube; aluminium alloy; Finite Element model; tube expansion test.

Abstract. The definitive implementation of Aluminium alloys as the main choice for lighter structural components needs the availability of innovative manufacturing processes capable of overcoming their poor formability at room temperature. The local modifications of the material properties (by means of short-term heat treatments) have shown their effectiveness in such terms. In a previous study from the same authors, it was experimentally investigated that, if a AA6063-T6 tubular component is locally brought to the overaged condition, its strain behavior significantly changes during an expansion test with elastomer. In light of this, the equipment used for the tube expansion tests was simulated by means of a FE model created using Abaqus and properly tuned using data coming from experimental tests carried out on AA6063-T6 tubular specimens. The calibrated model could be thus used to simulate the tube expansion while considering several distributions of the material properties (obtained through different heating strategies). Numerical results confirmed the possibility to change the slope of the strain path, thus suggesting that the strain behavior of a tubular component can be tailored, according to the specific applications, by properly designing the laser heating strategy.

Introduction

The current normative framework in terms of harmful emissions is imposing a dramatic reduction of fuel consumption for the transportation sector in general [1]. The research for solutions able to tackle such an issue is still open: it has been widely recognized that the reduction of the vehicle masses is one of the most direct solutions to reduce pollution [2]. Nevertheless, the same standards of passengers' comfort as well as safety must be ensured [3]. In light of this, the scientific community has focused its attention on the definition of new products able to combine limited weight, good level of strength, and high standard of safety. Aluminum (Al) and its alloys are regarded as ideal candidates to match all the mentioned requirements: in particular, especially for the automotive sector, the adoption of tubular components (especially for the structural purposes) have shown several advantages since they can combine the necessary stiffness without excessively increasing the vehicle's weight.

The promising outcomes that can be reached by massively adopting Al alloys for structural components are partially counterbalanced by its poor formability at room temperature [4]. Therefore, in order to get the desired complexity, innovative manufacturing routes have been investigated. Among the others, the approach based on the local modification of the material properties by means of a short-term heat treatment has demonstrated huge potentialities [5]: in fact, the resulting distribution of strength/ductility is capable of enhancing the material formability at room temperature. Moreover, since the approach is based on the material deformation at room temperature, the costs related to the equipment are sensibly reduced.

Literature confirms the effectiveness of the mentioned approach especially when applied to sheet metal parts [6,7], whereas only few examples deal with the possibility to apply a local modification to tubular components [8]. In a previous work, the authors investigated experimentally the effect of

laser treatments on the formability of AA6063 tubular samples subjected to expansion tests with elastomer [9]: in particular, tubes in the T6 conditions were heated by means of a CO_2 laser beam, along linear tracks parallel to the tube axis, to locally bring the material in the overaged state. Experimental tests demonstrated that the presence of a gradient of material properties altered appreciably the behavior within the deformation zone, not only in terms of ultimate fracture strain but also in terms of the evolution of the strain path. According to these results, the purpose of this work is to reproduce the tube expansion test within a CAE environment in order to numerically investigate possible strategies of local modification to evaluate how the different strategy can have an influence on the material strain behaviour.

Material and Methodology

Material. The alloy under investigation belongs to the group of the age-hardenable Al alloys (AA6063). The T6 condition was considered as the reference one; Table 1 lists the chemical composition of the investigated alloy.

Table 1 AA6063-T6: chemical composition (the content of alloying elements is expressed in wt%)

Al	Si	Cu	Fe	Mg	Mn [%]	Cr%]	Ti [%]	Zn [%]
Bal.	0.2-0.6	<0.1	<0.35	0.45-0.9	<0.1	<0.1	<0.1	<0.1

Numerical Analysis. The experimental setup adopted for the tube expansion tests, detailed in [10], was reproduced within the CAE environment of the Finite Element (FE) commercial code Abaqus. For the sake of clarity, a schematic representation of the setup is reported in Figure 1 [10].

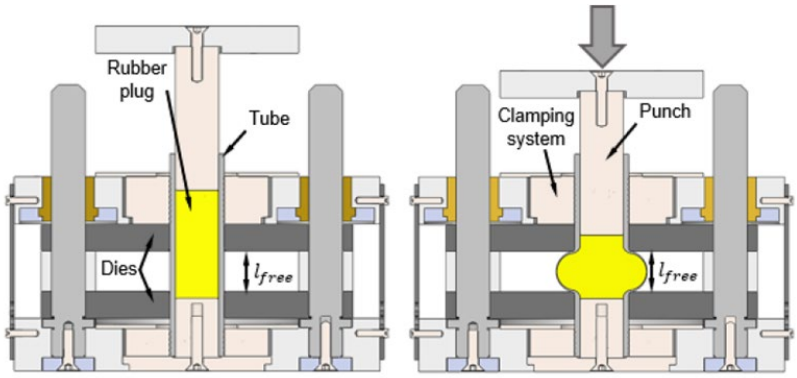

Figure 1 Schematic representation of the tube expansion test [10]

The tube is clamped between the two dies that are reciprocally positioned to define a specific value of the free length (l_{free} in Figure 1); the punch stroke compresses the rubber plug (highlighted in yellow) which, in turn, makes the tube deform within the defined free length.

To evaluate how the local modification of the material properties could have an influence on the tube's strain behaviour within the deformation zone, it was at first necessary to build up an accurate and reliable FE model able to reproduce the experimental material behaviour. The methodology proposed in this work, as shown in Figure 2, can be regarded as a double-step based approach: in the first step, a light 2D axisymmetric model was used to calibrate the friction coefficients describing the contact pairs between tube, rubber and tools. The so-determined coefficients were then transferred to the second model (created according to a 3D approach) to evaluate the effect of different distributions of properties on the nodal strain paths from the tube deformation zone.

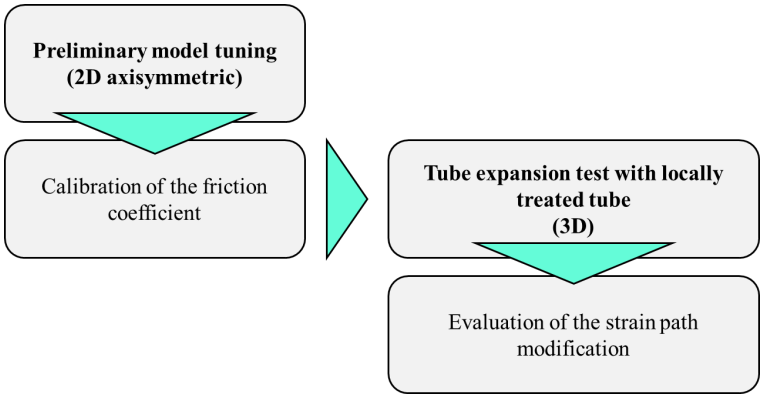

Figure 2 Schematic description of the adopted methodology

Tuning of the FE model. The first step was mainly aimed at tuning the FE model: more in details, the coefficient of friction between the rubber plug and the tube was inversely determined by minimizing the difference with the loading curve acquired during the experimental tests. Moreover, it was also checked that the deformation region was characterized by a strain evolution close to the plane strain condition. To effectively tune the numerical mode, a 2D axisymmetric approach – characterized also by a limited computational cost – was taken into account. The representation of the modelled assembly is shown in Figure 3a.

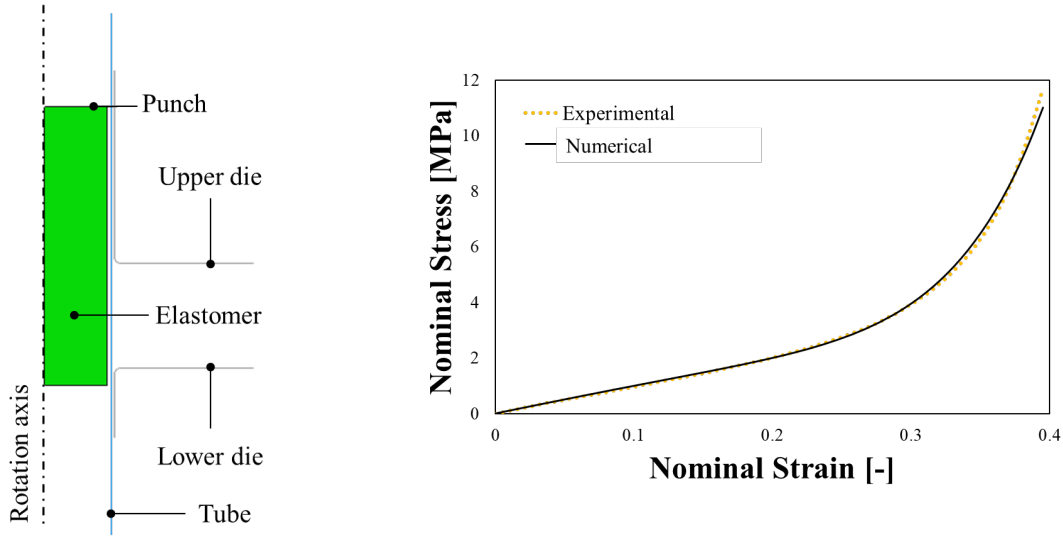

a) b)

Figure 3 FE model: a) 2D axisymmetric approach; b) calibration of the constitutive equation for the elastomer

The tools (upper and lower dies, as well as the punch) were modelled as wire-based analytical rigid bodies (no need for subsequent discretization), whereas the elastomer and the tube (150 mm long, outer diameter of 40 mm, initial thickness of 2 mm) as deformable bodies. Numerical simulations were run considering the tube fully in the condition as-purchased (T6), thus implementing the data reported in [10]. The J2 plasticity formulation (isotropic Von Mises) was taken into account as the material model. Moreover, a FLD-based damage criterion was also activated by implementing the forming limit curve that was analytically calculated according to the methodology described in [11]. The tube was discretized by 300 SAX1 elements (2-node linear shell with an average size of 0.5 mm).

The rubber, on the other hand, was treated as an hyperelastic material and its behaviour was modelled according to the Ogden's model [12]. The constants of the constitutive equation were inversely calculated using an internal Abaqus subroutine that minimized the error with data coming from an experimental rubber compression test, carried out according to the reference standard [13]. The geometry was meshed with 5760 CAX4RH elements (4-node bilinear, reduced integration with hourglass control, hybrid formulation, with an average size of 1 mm).

Tube expansion with locally treated tubes. The calibrated friction coefficients were subsequently used to define the interaction properties contact pairs in the second FE model, created according to a 3D approach. Such a choice was, in fact, due to the need of modelling certain material distributions that could not be simulated under the axisymmetric approach. Similarly, to the 2D model, the tools were modelled as discrete rigid shell bodies, whereas the tube (same geometry detailed in the 2D approach) and the rubber plug as deformable one. Also for the 3D approach, the J2 plasticity formulation was taken into account as the material model. The modelled assembly is shown in Figure 4 (the transparent view has been chosen for the sake of clarity): also for the second model, the free length of 30 mm was considered.

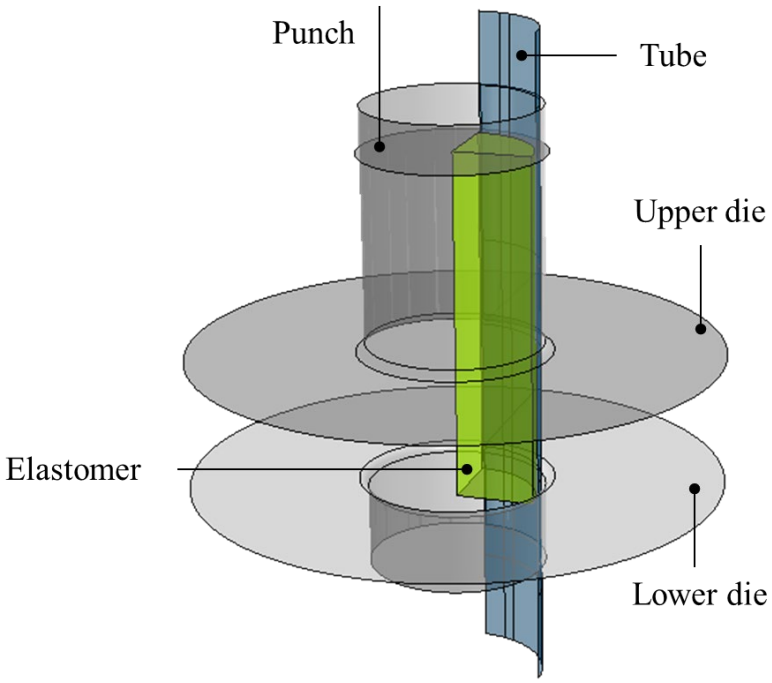

Figure 4 FE 3D model: assembly

The second set of numerical simulations were run considering the tube as already subjected to the laser heating, thus already characterized by the resulting distribution of T6 and overaged regions. To do this, the material behaviour was modelled implementing the flow curves in both the T6 (grey curve in Figure 5a) and overaged conditions (green curve in Figure 5a, taken from [9]). Also for this second model, a FLC-based damage criterion was activated by implementing the two limit curves (one for each for condition), analytically calculated from the two stress curves [11] (see Figure 5b).

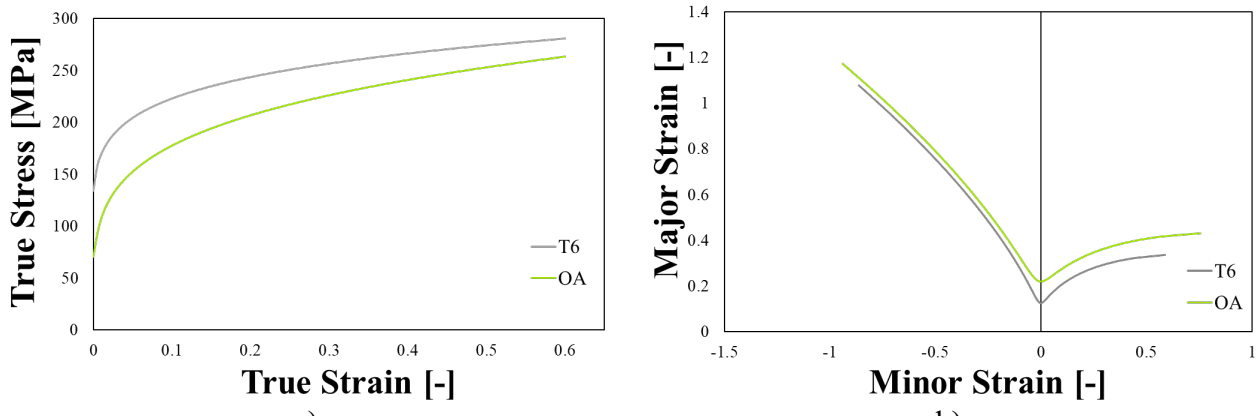

Figure 5 The implemented material data regarding both the conditions of interest: a) flow curves, b) forming limit curves

The implemented material data were then assigned to the correspondent tube's regions by means of a field variable: in such a way, properties in the overaged condition could be always assigned to the regions that were supposed to be irradiated by the laser (green regions in Figure 6), whereas the remaining part could be modelled in the T6 state (grey regions in Figure 6). In order to make the simulation more accurate, a transition region (extent of 2.5 mm) was also taken into account, in which the material properties were modeled as intermediate between the T6 and the overaged conditions (violet regions in Figure 6).

More in details, four different properties distribution were investigated: (i) the *AH* (*Axial Heating*) distribution, resulting from a heating strategy based on linear tracks, every 90 degrees, running parallel to the tube axis (Figure 6a); (ii) the *HH* (*Hoop Heating*) distribution, resulting from a heating strategy based on two circumferential tracks located in correspondence of both the dies entry radius (Figure 6b); (iii) the *MSH* (*Middle Spot Heating*) distribution, resulting from a heating strategy based on single discrete spots, every 90 degrees, located in the middle of the tube deformation zone (Figure 6c); (iv) the *CSH* (*Corner Spot Heating*) distribution, resulting from a heating strategy based again on single discrete spots, every 90 degrees, located in correspondence of both the dies entry radius (Figure 6d).

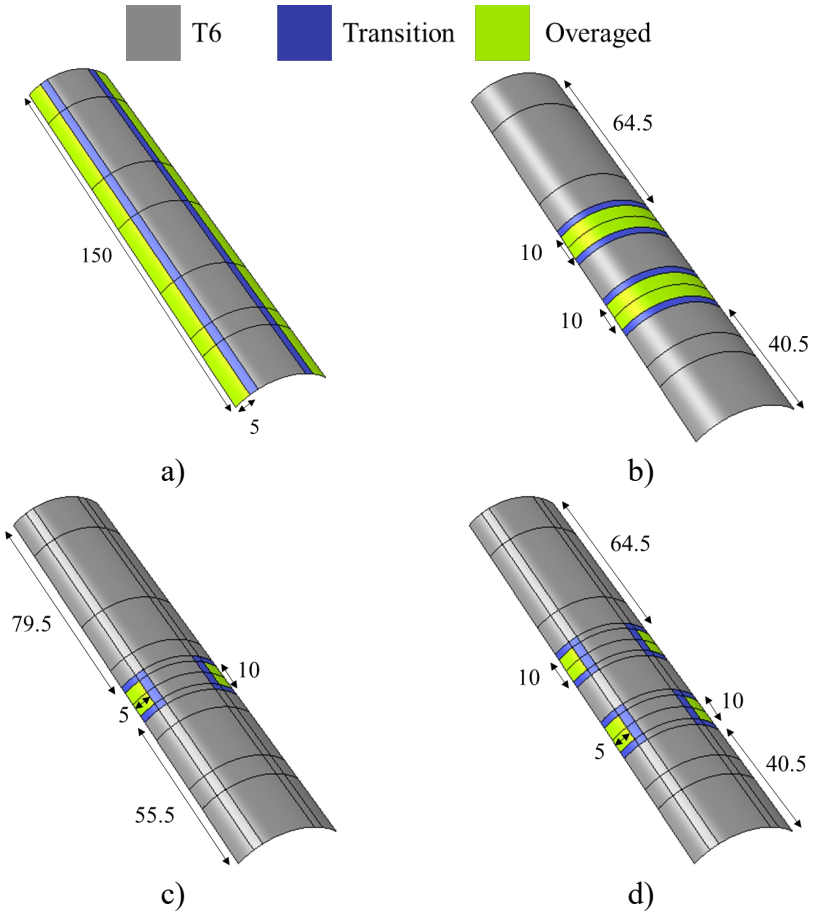

Figure 6 Effect of the investigated laser heating strategies in terms of properties distribution: a) AH, b) HH, c) MSH, d) CSH

Results and Discussion

Tuning of the friction coefficient. As described in the previous section, the adoption of a 2D axisymmetric approach came from the need to preliminarily determine some unknown quantities, as for example the friction coefficients defining the contact pairs between the tube, the rubber and the tools. The definition of those coefficients was achieved by minimizing the difference between the experimental load applied by the punch during the experimental test and the corresponding numerical curve.

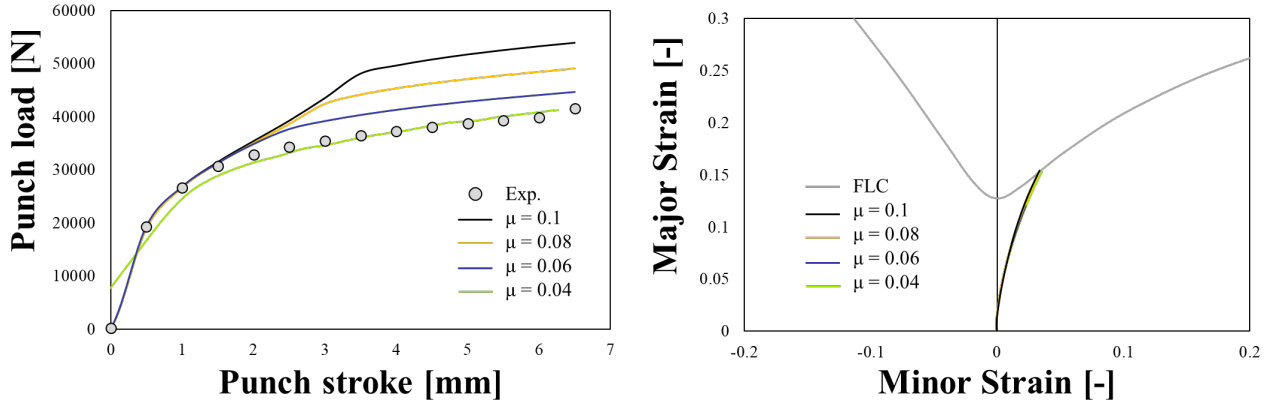

Figure 7 First-step FE simulation: a) calibration of the tube-rubber friction coefficient; b) effect of the friction coefficient on the strain path

Figure 7a confirms the good level of correspondence between the numerical and experimental load curve when the friction coefficient at the tube-rubber contact pair was set to 0.04. The experimental load curve (grey dots) is plotted up to the punch stroke equal to 6.5 mm, which corresponds to the moment at which the fracture of the tube occurred in the experimental test. At the same time, the implementation of the FLC curve made possible the numerical determination of the rupture occurrence, i.e. when the FLDCRT output variable [15] overcame the threshold value of 1 (basically it estimates how close is the nodal strain with respect to the limit condition). The numerical curves are consequently plotted in Figure 7a up to the time instant at which the model predicted the occurrence of fracture of the tube, thus further confirming the accurateness of the numerical results.

Such considerations were also strengthened by looking at the strain path extracted from the node located in the middle of the tube deformation zone (Figure 7b): all the strain paths are plotted up to the time instant before the occurrence of fracture and, as expected, are below the limit described by the forming limit curve (grey curve in Figure 7b). Moreover, it is quite evident that the friction coefficient has a negligible effect on the strain path evolution, which remains to be quite close to the plane strain conditions in accordance with what was reported in [10].

Effect of the heating strategy on the strain behavior. Results from the numerical runs when simulating the tube as already subjected to the local laser heating were preliminarily analyzed in terms of distributions of the FLDCRT output, shown in Figure 8. All the tube regions highlighted in grey refer to zones where the model predicted the fracture, i.e. where the FLDCRT variable overcame the threshold limit equal to 1.

As it can be seen, fracture was predicted in the tube portion kept in at the T6 condition when both the *HH* (Figure 8b) and the *CSH* strategies (Figure 8d) were adopted; on the other hand, a more severe strain condition – i.e. higher values of the FLDCRT variable – was reached in the overaged regions for the other two investigated strategies, *AH* (Figure 8a) and *MSH* strategies (Figure 8c).

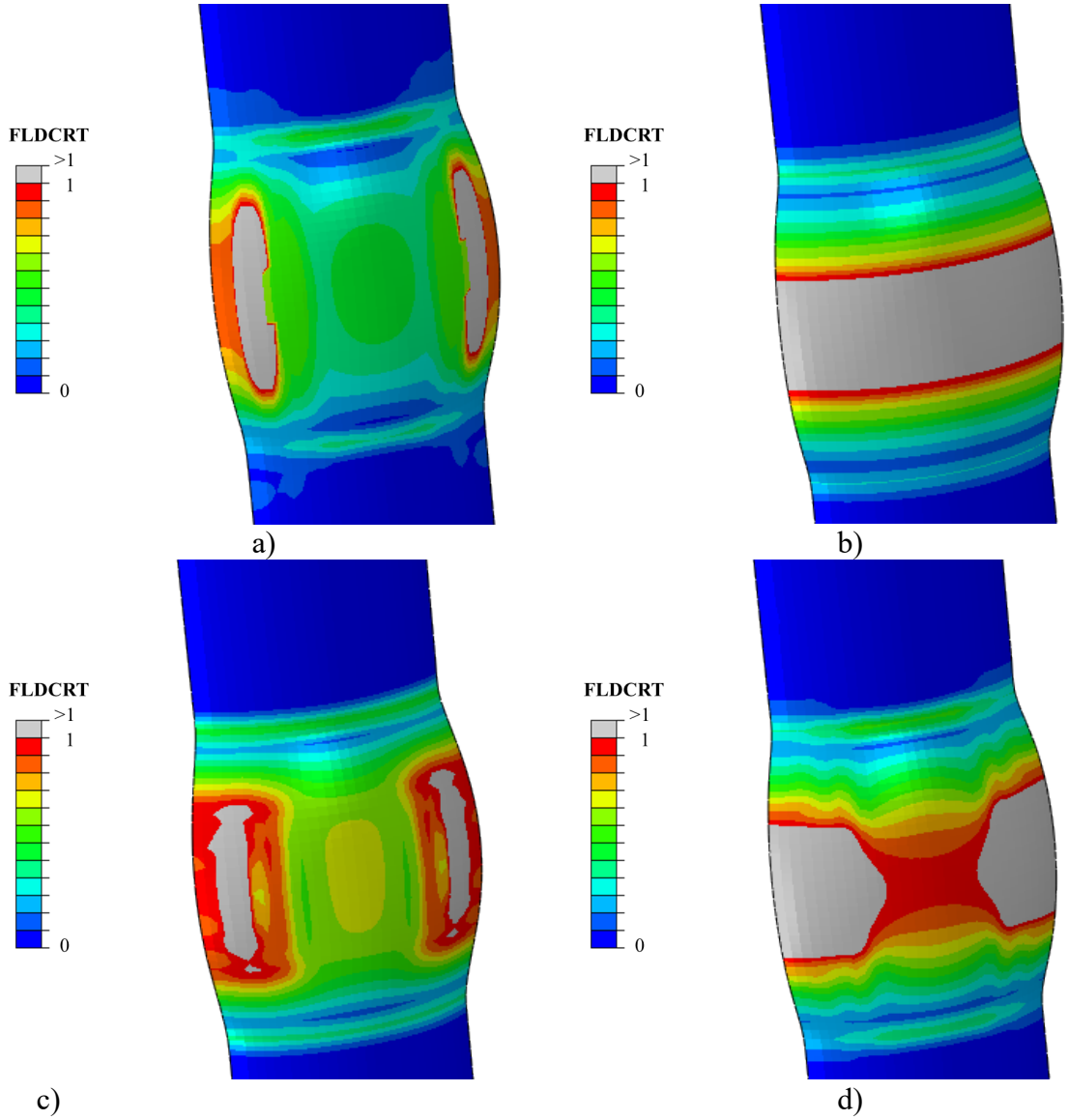

Figure 8 Final distribution of the FLDCRT variable: a) AH, b) HH, c) MSH and d) CSH

The evaluation of the effect of the heating strategy on the tube strain behaviour was completed by looking at the strain path extracted from a node approximately located at the center of the deformation zone shown in Figure 9.

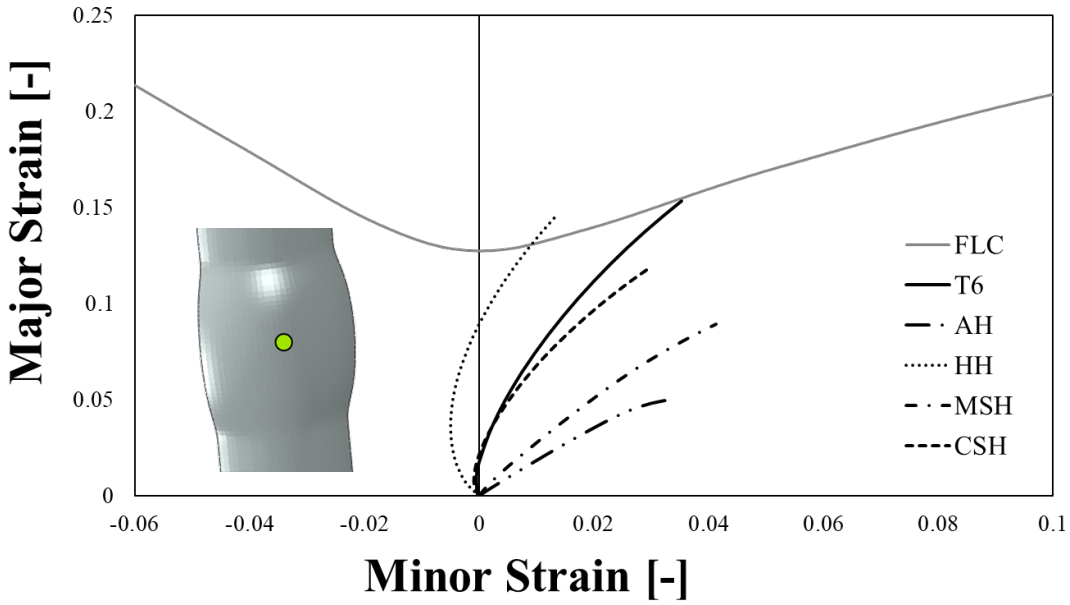

Figure 9 Influence of the heating strategy on the strain path of the indicated point

Strain paths from the four investigated conditions are plotted along with the FLC in the T6 state and the strain path concerning the expansion test of the tube in the T6 state (green curve). It can be easily noted that if the material properties within the deformation zone were altered (as in the case of the *AH* and *MSH* strategies), the slope of the strain path sensibly changed, and the monitored node exhibited a strain condition close to the biaxial state rather than to the plane strain one.

On the other hand, if the local modification was achieved in the proximity of the tube region in contact with the dies entry radius, the strain path's change resulted to be less evident: the *CSH* strategy, in fact, was characterized by a strain condition quite close to the one in absence of any local heating. The *HH* strategy, despite showing an initial strain path characterized by negative minor strains, tended to curve back toward a strain evolution close to the one of the tube in the T6 state.

Another interesting consideration could also be drawn by analyzing how the specific heating strategy had an influence on the punch load-stroke curve: as shown in Figure 10, the wider the extent of the overaged portion of the deformation zone was, the lower load the punch had to apply to deform the tube. Moreover, irrespective of the specific local heating strategy, the presence of the overaged zones led to a sensibly lower values of the punch load (the peak value after 6.5 mm of stroke) around 10 kN (one quarter of the peak value reached before rupture during the expansion test with the AA6063-T6 tube).

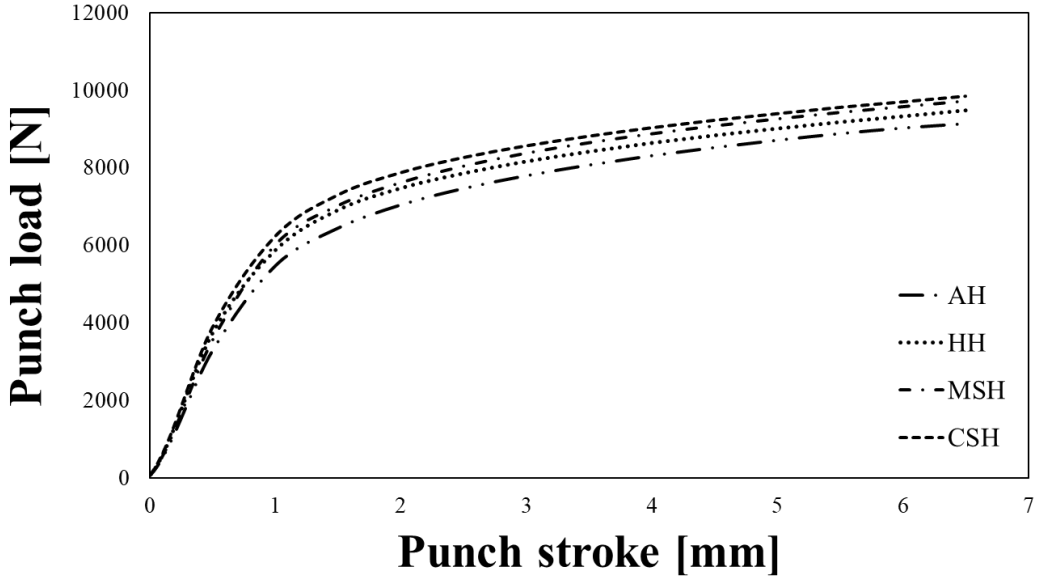

Figure 10 Effect of the heating strategies on the punch load-stroke curve

Conclusions

In the present work, a two-step numerical methodology has been presented to evaluate the effect of different heating strategies on the strain behaviour of a tubular component during the expansion test with elastomer.

The inverse calibration of the friction coefficient, carried out in the first step of the proposed methodology, was necessary to build up a 3D model accurate enough to evaluate the effect of the different distributions of properties (as a consequence of different laser heating strategies) on the evolution of the strain paths extracted from the tube deformation zone.

The FLDCRT maps combined with the evolution of the strain condition extracted from the center of the deformation zone suggested that a more evident change in the slope of the strain path was obtained when the local modification of the material properties interested the deformation zone. On the other hand, if the material properties were modified in the tube region in contact with the dies entry radius, the change in the strain path resulted to be less evident and, as a consequence, the strain evolution was closer to the one obtained in the fully T6 state.

Results from the second set of numerical simulations demonstrated that, by changing the heating strategies, the material's strain behaviour can be tailored accordingly. In such a way, the proposed approach can be used to manufacture tubular components for transport application able, for example, to combine strength and crashworthiness thanks to the optimized distribution of properties. The next steps will be focused on carrying out the experimental expansion tests with elastomer adopting tubes, whose properties have been locally modified according to the discussed strategies, to validate the numerical results.

References

[1] Mayer, R. M., Poulikakos, L. D., Lees, A. R., Heutschi, K., Kalivoda, M. T., and Soltic, P., 2012, "Reducing the Environmental Impact of Road and Rail Vehicles," Environ. Impact Assess. Rev., **32**(1), pp. 25–32.

[2] Hirsch, J., 2014, "Recent Development in Aluminium for Automotive Applications," Trans. Nonferrous Met. Soc. China (English Ed., **24**(7), pp. 1995–2002.

[3] DIN EN 45545-2, 2016, "Railway Applications - Fire Protection on Railway Vehicles - Part 2: Requirements for Fire Behaviour of Materials and Components."

[4] Kalpakjian, S., and Schmid, S. R., 2017, *Manufacturing Processes for Engineering Materials*, Pearson Education, Singapore; London.

[5] Geiger, M., Merklein, M., and Vogt, U., 2009, "Aluminum Tailored Heat Treated Blanks," Prod. Eng., **3**(4–5), pp. 401–410.

[6] Piccininni, A., and Palumbo, G., 2020, "Design and Optimization of the Local Laser Treatment to Improve the Formability of Age Hardenable Aluminium Alloys," Materials (Basel)., **13**(7).

[7] Kahrimanidis, A., Lechner, M., Degner, J., Wortberg, D., and Merklein, M., 2015, "Process Design of Aluminum Tailor Heat Treated Blanks," Materials (Basel)., **8**(12), pp. 8524–8538.

[8] Peixinho, N., Soares, D., Vilarinho, C., Pereira, P., and Dimas, D., 2012, "Experimental Study of Impact Energy Absorption in Aluminium Square Tubes with Thermal Triggers," Mater. Res., **15**(2), pp. 323–332.

[9] Piccininni, A., Magrinho, J. P., Silva, M. B., and Palumbo, G., 2021, *Formability Analysis of a Local Heat-Treated Aluminium Alloy Thin-Walled Tube*, Springer International Publishing.

[10] Magrinho, J. P., Silva, M. B., Centeno, G., Moedas, F., Vallellano, C., and Martins, P. A. F., 2019, "On the Determination of Forming Limits in Thin-Walled Tubes," Int. J. Mech. Sci., **155**(March), pp. 381–391.

[11] Mattiasson, K., Sigvant, M., and Larsson, M., 2006, "Methods for Forming Limit Prediction in Ductile Metal Sheet," *IDDRG'06 Proceeding*.

[12] Ogden, R. W., 1997, *Non-Linear Elastic Deformations*, Dover Publications.

[13] ASTM, 2019, "D575 - Standard Test Methods for Rubber Properties in Compression," **91**(Reapproved 2018), pp. 1–4.

[14] Magrinho, J. P., Centeno, G., Silva, M. B., Vallellano, C., and Martins, P. A. F., 2019, "On the Formability Limits of Thin-Walled Tube Inversion Using Different Die Fillet Radii," Thin-Walled Struct., **144**(July).

[15] Dassault Systems, 2017, "Abaqus Analysis User's Manual."